Kinetic Model for FGF, FGFR, and Proteoglycan Signal Transduction Complex Assembly†

Omar A. Ibrahimi,‡ Fuming Zhang,§ Sybil C. Lang Hrstka,+ Moosa Mohammadi,‡ and Robert J. Linhardt*,§,+

Department of Pharmacology, New York University School of Medicine, New York, New York 10016, Departments of Chemistry, Biology, and Chemical Engineering, Rensselaer Polytechnic Institute, Troy, New York 12180, and Chemical and Biochemical Engineering, University of Iowa, Iowa City, Iowa 52242

Received July 14, 2003; Revised Manuscript Received January 26, 2004

ABSTRACT: The current working model for fibroblast growth factor receptor (FGFR) dimerization and activation requires the assembly of a ternary complex of fibroblast growth factor (FGF), FGFR, and heparin or heparan sulfate proteoglycan (HSPG) on the plasma membrane. The recent FGF2−FGFR1−heparin crystal structure provides a detailed but static view of the FGF−FGFR−heparin complex. However, the kinetics of ternary complex assembly has yet to be investigated. Here, we characterize FGF2, FGFR1, and heparin interactions using surface plasmon resonance (SPR). Binding constants for binary FGF2/FGFR1 (K_D = 62 nM), FGF2/heparin (K_D = 39 nM), and FGFR1/heparin (K_D = 3.2 μM) interactions correlate to the magnitude of binding interface observed in the FGF2−FGFR1−heparin crystal structure. Interestingly, comparison of sensorgrams of sequential injections of FGF2 and FGFR1 and equimolar FGF2−FGFR1 injections onto a heparin neoproteoglycan surface demonstrates that FGF2 dramatically enhances the association of FGFR1 with heparin and leads us to propose a model for the stepwise assembly of a ternary FGF−FGFR−HSPG complex. The weak binding affinity of the FGFR1−heparin interaction suggests that in this model, FGFR and HSPG are unbound in the absence of FGF ligand. The availability of FGF results in formation of initial FGF−HSPG complexes, which promotes the rapid binding of FGFR and creates a ternary complex capable of undergoing dimerization and subsequent FGFR activation. In contrast, alternative models for the kinetic assembly of a ternary complex in which binary FGF−FGFR or FGFR−HSPG complexes are intermediates do not conform well with the experimental data.

The fibroblast growth factor (FGF) family consists of 22 structurally related proteins with pleiotropic signaling activities (*1*). Each FGF consists of a core region of homology of 100−120 residues known as a β-trefoil core, in addition to variable N- and C-terminal regions. The biological responses to the FGF ligand are mediated by one of four receptor tyrosine kinases, FGFR1−4. Each FGFR is composed of an extracellular ligand-binding region comprised of three immunoglobulin (Ig)-like domains (D1-D3), a single transmembrane helix, and a cytoplasmic segment with tyrosine kinase activity. The minimal portion of the extracellular domain necessary for ligand binding and specificity is D2, D3, and the interconnecting linker. Alternative splicing of the second half of D3 in FGFR1−3 extends the number of functional FGFRs to seven and plays a central role in determining ligand-binding specificity (*2*−*5*).

Receptor dimerization is a central step in FGFR activation and requires heparin or heparan sulfate proteoglycans (HSPGs), in addition to ligand binding (*4*, *6*−*8*). The recent crystal structure of a dimeric 2:2:2 FGF2−FGFR1−heparin ternary complex has provided a mechanistic view by which FGF, FGFR, and HSPG cooperate to promote FGFR dimerization (*9*). In this two-end model, two 1:1:1 FGF−FGFR−heparin ternary complexes associate to form a symmetrical dimer. Within the dimer, each FGF binds to both receptors, and the two receptors interact with one another as well. Within each 1:1:1 ternary complex, heparin interacts extensively with FGF and FGFR, thereby augmenting FGF−FGFR affinity. Moreover, heparin from one 1:1:1 ternary complex interacts with the FGFR of the adjoining 1:1:1 ternary complex. Hence, heparin plays a dual role by increasing FGF−FGFR affinity and also by promoting the dimerization of two 1:1:1 ternary complexes by stabilizing protein−protein contacts between the two ternary complexes (*9*). A recent study independently supports a 2:2:2 FGF/FGFR/heparan sulfate binding stoichiometery using biochemical methods (*10*), although an alternative dimerization model has also been proposed based on the crystal structure of a dimeric 2:2:1 FGF1−FGFR2−heparin complex (*11*).

While the ternary crystal structure of FGF2−FGFR1-heparin has provided detailed insights into the nature of FGF, FGFR, and heparin interactions, the dynamics of FGF−FGFR−heparin complex assembly has not yet been investigated. To address this question, we have applied surface

† We thank the National Institutes of Health for sponsoring this research in the forms of Grants HL52622 (R.J.L.) and DE13686 (M.M.).

* To whom correspondence should be addressed. Phone: (518) 276-3404. Fax: (518) 276-3405. E-mail: linhar@rpi.edu.

‡ New York University School of Medicine.

§ Rensselaer Polytechnic Institute.

+ University of Iowa.

10.1021/bi0352320 CCC: $27.50
Published on Web 03/30/2004

plasmon resonance (SPR) to study the kinetics of FGF, FGFR, and heparin interactions. Here, we report the kinetic constants for FGF2/FGFR1, FGF2/heparin, and FGFR1/heparin interactions. Moreover, the ability of SPR to monitor interactions in real time permits us to construct a model for FGF−FGFR−heparin assembly based on sequential injections of FGF2 and FGFR1 and equimolar FGF2−FGFR1 injections onto a surface containing immobilized heparin neoproteoglycan.

MATERIALS AND METHODS

Protein Expression and Purification. The ligand-binding portion of human FGFR1 (IIIc spliceform) consisting of D2-D3 (residues 142−365) was prepared as previously described (*12*). Full-length human FGF2 (residues 1−155) was purified according to a previously reported protocol (*13*). FGF homologous factor 1b (FGF12b), a protein structurally related to FGFs that does not bind FGFRs, was expressed and purified as previously described (*14*). Purified FGFR1, FGF2, and FHF1b were concentrated using a Centricon-10 (Millipore, Billerica, MA) centrifugal microultrafiltration tube. Protein concentrations were determined by measuring the UV absorption spectrum using a Beckman DU640B spectrophotometer (Beckman Coulter, Fullerton, CA) for each purified protein in 6.0 M guanidium hydrochloride and 0.02 M sodium phosphate buffer (pH = 6.5). Absorbance at 280 nm was used with the extinction coefficient, determined using the ProtParam tool (http://us.expasy.org/tools/protparam.html) at that wavelength to calculate concentration. The protein stock concentrations are as follows: FGFR1 (12.5 μM), FGF2 (480 μM), and FHF1b (61 μM).

Preparation of Neoproteoglycan and FGF Sensor Chips. Neoproteoglycan sensor chip was made by covalently immobilizing albumin−heparin conjugate (Sigma, St. Louis, MO), prepared by coupling heparin's terminal formyl group to bovine serum albumin through reductive amination, to the C1 biosensor chip through amine coupling (Biosensor AB, Uppsala, Sweden) (*15*). There are approximately 80 free amino groups in albumin as compared to a single free amino group in each heparin chain. Thus, the probability of free amino groups in heparin, which have markedly diminished nucleophilicity, reacting with the activated chip surface is very low. Carboxymethyl groups on the C1 chip surface were first activated using an injection pulse of 50 μL (flow rate, 5 μL/min) of an equimolar mix of *N*-ethyl-*N*-(dimethyaminopropyl) carbodiimide (EDC) and *N*-hydroxysuccinimide (NHS) (final concentration 0.05 M, mixed immediately prior to injection). An albumin−heparin solution (200 μg/mL in sodium acetate buffer with 2 M guanidium hydrochloride, pH 4.0) was applied to the activated chip surface. This buffer was selected to increase the coupling efficiency of the heparin-albumin conjugate. Excess unreacted sites on the sensor surface were deactivated with a 40 μL injection of 1 M ethanolamine. Successful immobilization was confirmed by the observation of a ∼300 response unit (RU) increase. The control flow cell was prepared by immobilizing bovine serum albumin using a similar coupling procedure.

The FGF sensor chip was prepared by immobilization of FGF2 (ΔRU ∼1000) on a research grade CM 5 chip (Biosensor AB, Uppsala, Sweden) through its primary amino groups using EDC/NHS according to standard amine coupling protocol (*16*). Following activation with EDC/NHS, successful immobilization of FGF2 was achieved by diluting FGF2 to 25 μg/mL in HBS-EP buffer (0.01 M HEPES, 0.15 M NaCl, 3 mM EDTA, 0.005% polysorbate 20 (v/v)), pH = 7.4. FGF12, an FGF that does not bind FGFRs, was immobilized on the reference flow cell as a control in a fashion similar to FGF2.

Measurement of FGF2/FGFR1, FGF2/Heparin FGFR1/Heparin, and FGF2−FGFR1/Heparin Interactions. Interactions were characterized using a BIAcore 3000 instrument (Biosensor AB, Uppsala, Sweden). For FGF2/FGFR1, FGF2/heparin, FGFR1/heparin, and FGF2−FGFR1/heparin interactions, different concentrations of analytes (FGF2 and/or FGFR1) in HBS-EP buffer were injected over the FGF2 sensor chip or the neoproteoglycan sensor chip at a flow rate of 50 μL/min. At the end of each sample injection (180 s), HBS-EP buffer was passed over the sensor surface to monitor the dissociation phase. Following 180 s of dissociation, the sensor surface was fully regenerated by injection of 50 μL of 2 M NaCl in 100 mM sodium acetate buffer (pH = 4). The kinetics of each binary interaction were negligibly affected by alterations in flow rate (1−100 μL/min) or the addition of glycerol (0.5−10 vol %) to the running buffer, thereby indicating that mass transport limitations were minimal (data not shown). Levels of nonspecific binding for each set of interactions were low and did not exceed 20% of the maximum RU value obtained for each interaction study.

For the FGF−FGFR−proteoglycan assembly experiments, different injection sequences of FGF and FGFR, or injection of 500 nM of FGF−FGFR complex, were used over the neoproteoglycan sensor chip. The time lag between the first and second injections in the sequential injection experiments was due to limitations in the BIAcore instrument.

Analysis of FGF2/FGFR1, FGF2/Heparin, and FGFR1/Heparin Binary Interactions. Reference responses from control flow cells, containing immobilized FGF12 or albumin, were subtracted from FGF2 or heparin−albumin flow cells, respectively, for each analyte injection using BiaEvaluation software (Biacore AS, Uppsala, Sweeden). The resulting sensorgrams were used for kinetic parameter determination by globally fitting the experimental data to a 1:1 interaction. A term was added for biosensor related effects when appropriate (BIAevaluation software, version. 3.1, 1999). χ^2 did not exceed 10% of R_{max} for each fit.

Analysis of FGF2−FGFR1/Heparin Interaction. Kinetic rate constants, association rate (k_a), and dissociation rate (k_d), obtained from FGF2/FGFR1, FGF2/heparin, and FGFR1/heparin binary interactions, served as initial values for determining the apparent kinetic parameters of the FGF2−FGFR1/heparin interaction. The equilibrium constant (K_D) determined from the FGF2/FGFR1 binary interaction study was used to calculate solution concentrations of FGF2, FGFR1, and FGF2−FGFR1 in the injected samples. Apparent kinetic parameters from the equimolar FGF2−FGFR1 injection studies were calculated by deriving a set of ordinary differential equations to model the various species interacting at the sensor chip surface. At the three lowest solution concentrations of FGF2−FGFR1, the binding of each species

to heparin could be precisely determined. The following equations were derived to model these interactions:

$$\frac{d[H]}{dt} = -(k_{a_1}[F][H] - k_{d_1}[FH]) - (k_{a_2}[FR][H] - k_{d_2}[FRH]) \quad (1)$$

$$\frac{d[FH]}{dt} = (k_{a_1}[F][H] - k_{d_1}[FH]) - (k_{a_3}[R][FH] - k_{d_3}[FRH]) \quad (2)$$

$$\frac{d[FRH]}{dt} = (k_{a_2}[FR][H] - k_{d_2}[FRH]) + (k_{a_3}[R][FH] - k_{d_3}[FRH]) \quad (3)$$

The abbreviations are as follows: heparin [H], FGF2 [F], FGFR1 [R], FGF2−FGFR1 [FR], and FGF2−FGFR1−heparin ternary complex [FRH]. The data were reevaluated for possible mass transfer limitations by incorporating an additional term for mass transfer in the ordinary differential equations. Estimation of the mass transfer coefficient, k_M, was found to be considerably lower than the product of association constant and the sensor surface receptor concentration for each interaction, which is suggestive of reaction-rate-limited interactions (*17*). When higher solution concentrations of equimolar FGF2−FGFR1 were injected, several additional interactions became important, such as dimerization, thereby introducing a degree of complexity that could not be accurately modeled and were outside the scope of this study.

RESULTS

On the basis of the two-end dimerization model, we envision three possible models for the stepwise assembly of a ternary FGF−FGFR−HSPG complex (Figure 1). In the absence of FGF ligand, FGFR and HSPG can exist in either an unassociated state (a in models 1 and 2) or an associated state (b in model 3). The presence of FGF can result in initial complexes of either FGF−HSPG (c in model 1), FGF-FGFR (d in model 2), or FGF−FGFR−HSPG ternary complex (e in model 3). The formation of binary FGF−HSPG or FGF−FGFR complex (c and d) is then followed by FGF−FGFR−HSPG ternary complex formation (e), and in biological systems, subsequent dimerization $(FGF-FGFR-HSPG)_2$ and activation (f).

FGF2/FGFR1, FGF2/Heparin, and FGFR1/Heparin Binary Interactions. To differentiate between these three models, we first measured the association rates (k_a), dissociation rates (k_d), and dissociation constants (K_D) for binary interactions occurring between FGF2 and FGFR1, FGF2 and heparin, and FGFR1 and heparin (Figure 2A−C). The strongest binary interaction observed was the FGF2/heparin interaction (39 nM), followed by the FGF2/FGFR1 interaction (62 nM) and the relatively weak FGFR1/heparin interaction (3.2 μM) (Table 1). A potential caveat of the FGF2/heparin binding data is that saturation is not observed even at 10 × K_D and is suggestive that at higher concentrations of FGF2, the FGF2/heparin interaction is not 1:1.

The extent of FGF2−heparin and FGFR1−heparin interactions correlate with the amount of hydrogen bonds made, 16 and 9, respectively, in the FGF2−FGFR1−heparin crystal structure (*9*). Comparison of FGF2/heparin and FGFR1/heparin binding data to previous binding studies using optical biosensors reveals that dissociation constant values obtained for FGF2/heparin binding were similar (~10−90 nM) (*18*−*19*), whereas the value reported for dissociation constant of the FGFR1/heparin interaction (63 nM) (*20*) was roughly 5-fold lower. This difference in measurement can be attributed to the use of a dimeric form of FGFR1 by Powell et al., while our study employed a monomeric FGFR1. In contrast, the binding affinities for both interactions reported here are an order of magnitude stronger than the dissociation constants measured by ITC for each interaction (*21*). These differences in measurement may be attributed to the experi-

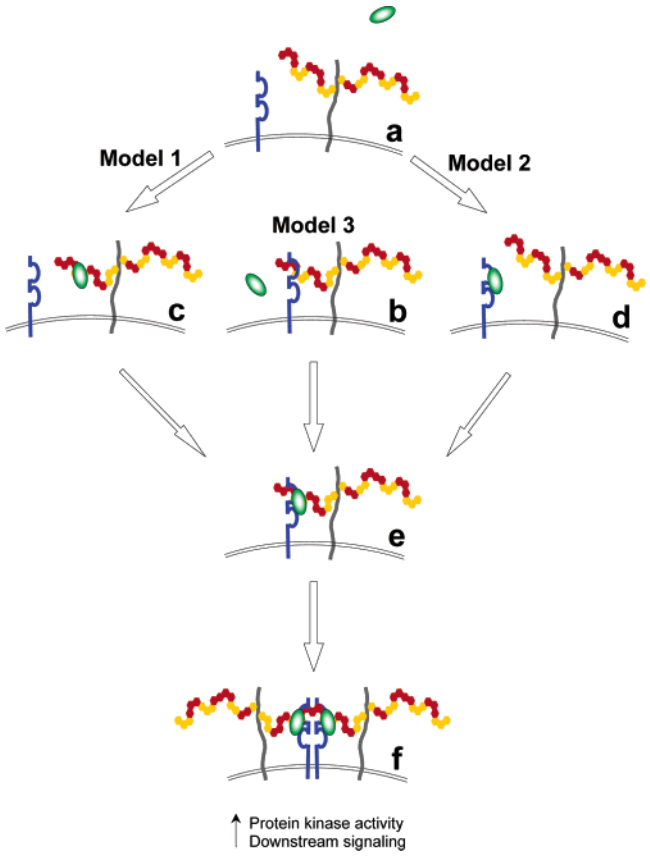

FIGURE 1: Models 2Op proposed for the stepwise assembly of an active FGF2−FGFR1−HSPG signaling complex at the cell surface. FGF2 is green; FGFR1 is blue; HSPG is red, yellow, and gray; and the cell membrane is represented by the slightly rounded double lines. Refer to text for a discussion of each model.

Table 1: Calculated Kinetic Parameters from the Various Interaction Studies

	k_a (M^{-1} s^{-1})	k_d (s^{-1})	K_D (M)
FGF2/FGFR1	$9.64 \times 10^4 \pm 8.06 \times 10^2$	$5.96 \times 10^{-3} \pm 5.84 \times 10^{-3}$	6.19×10^{-8}
FGF2/heparin	$1.1 \times 10^7 \pm 4.71 \times 10^5$	$0.43 \pm 1.92 \times 10^{-2}$	3.9×10^{-8}
FGFR1/heparin	$5.9 \times 10^3 \pm 3.1 \times 10^2$	$1.9 \times 10^{-2} \pm 8.23 \times 10^{-4}$	3.2×10^{-6}
FGF2/heparin [a]	144 ± 1.75	$1.18 \times 10^{-5} \pm 8.81 \times 10^{-7}$	8.21×10^{-8}
FGF2-FGFR1/heparin [a]	89.9 ± 1.55	$8.63 \times 10^{-3} \pm 9.45 \times 10^{-5}$	9.60×10^{-5}
FGF2-heparin/FGFR1[a]	$6.13 \times 10^3 \pm 4.67 \times 10^2$	$1.66 \times 10^{-5} \pm 1.26 \times 10^{-6}$	2.71×10^{-9}

[a] Values determined from the FGF2/FGFR1/heparin interaction study (Figure 3) using equations presented in the Materials and Methods.

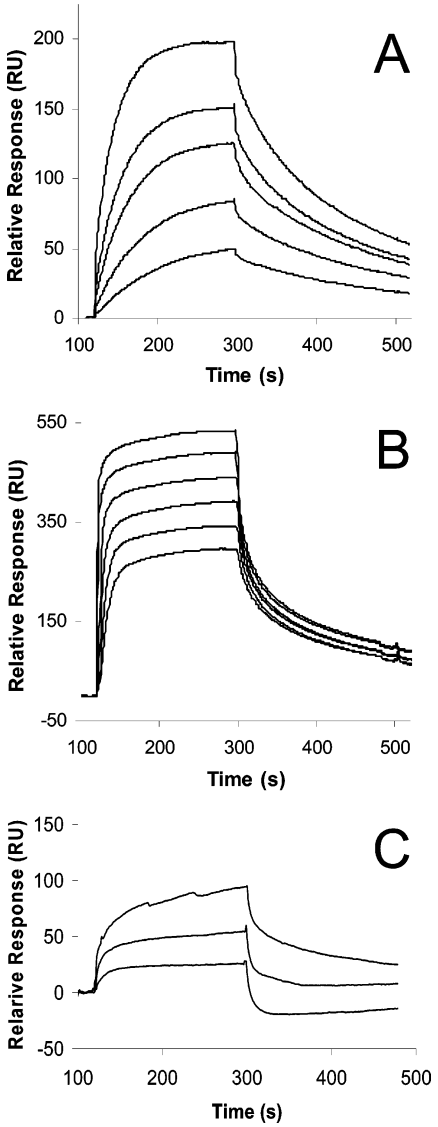

FIGURE 2: Panel A: interaction between FGF2 and FGFR1. Concentrations are 25, 50, 100, 200, and 400 nM. Panel B: interaction between FGF2 and heparin. Concentrations are 25, 50, 100, 200, 400, and 800 nM. Panel C: interaction between FGFR1 and heparin. Concentrations are 195 nM, 700 nM, and 12.5 μM.

mental system in which the interactions were studied. Measurements using ITC effectively characterize solution binding, whereas SPR measures binding in a two-phase system in which one of the interacting species is confined to a surface. Additionally, our study employed high molecular weight heparin (MW_{avg} ~12 kDa) in contrast to the low molecular weight heparin (MW_{avg} ~3 kDa) utilized in the ITC study (*21*). Analysis of FGF2 binding to baby hamster kidney-derived cells (BHK-21) yielded an apparent K_D of 270 pM (*22*). Covalent cross-linking of ^{125}I−FGF2 labeled two macromolecular species. Subsequent analysis of FGF2 binding to BHK-21 cells revealed high affinity and low affinity binding sites for FGF2 with K_D values of 20 pM and 2 nM, respectively (*23*). The high affinity site was initially proposed to represent FGFR, and the low affinity site represented cell-associated heparin molecules (*23*). Subsequent comparison of FGF2 binding to intact cells and also to each class of binding site in the absence of the other suggested that the high affinity binding site actually consisted of both FGFR and HSPG (*24*). The K_D value for the ternary FGF2−FGFR1−heparin complex (2.7 nM, Table 1) obtained in our study is 1−2 orders of magnitude weaker than the K_D values (~10−270 pM) obtained for FGF2 binding to high affinity sites on cells (*22*−*24*). The enhanced binding affinities observed in the cell binding assays likely reflect the increased stabilization of the ternary complex by dimerization, as each monomeric ternary complex in the dimeric assemblage contacts and stabilizes the adjoining ternary complex (*9*).

FGF2−FGFR1/Heparin Interaction. Next, the interaction between heparin and FGF2−FGFR1 complex was assessed by injecting equimolar mixtures of FGF2 and FGFR1 (Figure 3) at concentrations above and below the calculated K_D from the FGF2−FGFR1 interaction. These experiments provided further insight into heparin's interaction with different ratios of complexed FGF2−FGFR1 and free FGF2 and FGFR1. Ordinary differential equations were derived to model these data based on three distinct interactions: (1) FGF2 with heparin; (2) FGF2−FGFR1 with heparin; and (3) FGFR1 with an FGF2−heparin complex. There are three pathways to reach the ternary complex from a binary complex (Figure 1, pathways b−d). The first two, binary FGF2−heparin complex binding FGFR1 and binary FGF2−FGFR1 complex binding heparin, are modeled. The third pathway, FGFR1−heparin binding to FGF2, is unlikely due to the weak binding affinity of the FGFR1/heparin interaction and therefore not included in the modeling.

$$\text{FGF2} + \text{H} \underset{k_{d_1} = 1.18 \times 10^{-5}}{\overset{k_{a_1} = 144}{\rightleftharpoons}} \text{FGF2-H} \tag{4}$$

$$\text{FGF2}-\text{FGFR1} + \text{H} \underset{k_{d_2} = 8.63 \times 10^{-3}}{\overset{k_{a_2} = 89.9}{\rightleftharpoons}} \text{FGF2}-\text{FGFR1}-\text{H} \tag{5}$$

$$\text{FGF2-H} + \text{FGFR1} \underset{k_{d_3} = 1.66 \times 10^{-5}}{\overset{k_{a_3} = 6130}{\rightleftharpoons}} \text{FGF2}-\text{FGFR1}-\text{H} \tag{6}$$

DISCUSSION

Analysis of FGF2/FGFR1, FGF2/heparin, and FGFR1/heparin interactions and injections of equimolar FGF2−FGFR1 (Figures 2 and 3; Table 1) shows that model 1 best fits the experimental data, whereas models 2 and 3 are inconsistent with the data. Stepwise binding of the FGF2 ligand to HSPG followed by FGFR1 binding to the binary FGF2−HSPG complex, as depicted in model 1 (Figure 1, pathways a, c, and e), is consistent with the high binding affinity of the FGF2−heparin interaction (39 nM) (Table 1). The relatively high association rate ($k_a = 1.1 \times 10^7$ M^{-1} s^{-1}) of the FGF2/heparin interaction as compared to the association rates for FGF2/FGFR1 ($k_a = 9.64 \times 10^4$ M^{-1} s^{-1}) and for FGFR1/heparin ($k_a = 5.9 \times 10^3$ M^{-1} s^{-1}) favors the formation of an initial FGF2−heparin complex and suggests a mechanism for the rapid concentration of FGF ligand on the HSPG-containing plasma membrane (model 1). This concentration effect is probably physiologically relevant given the exceedingly low amounts of FGF involved in signaling (*25*). Moreover, binding of FGFR1 to binary FGF2−heparin complex (Figure 1, pathways c−e) in a heterogeneous mixture of FGF2, FGFR1, and FGF2−FGFR1 occurs nearly instantaneously ($k_a = 6130$ M^{-1} s^{-1}) when compared to binary FGF2−FGFR1 complex ($k_a = 89.9$ M^{-1}

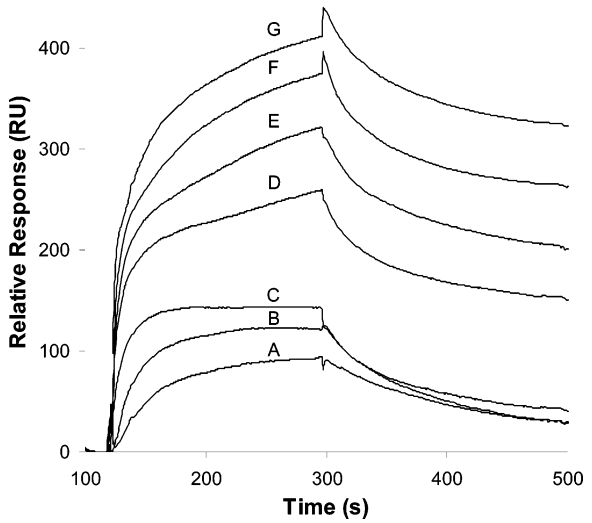

FIGURE 3: Binding curves obtained from increasing equimolar FGF2−FGFR1 injections. Concentrations of the species for each injection are (A) 7.0 nM FGF2, 7.0 nM FGFR1, and 0.8 nM FGF2−FGFR1; (B) 12.9 nM FGF2, 12.9 nM FGFR1, and 2.7 nM FGF2−FGFR1; (C) 22.8 nM FGF2, 22.8 nM FGFR1, and 8.4 nM FGF2−FGFR1; (D) 38.5 nM FGF2, 38.5 nM FGFR1, and 24.0 nM FGF2−FGFR1; (E) 62.3 nM FGF2, 62.3 nM FGFR1, and 62.7 nM FGF2−FGFR1; (F) 97.2 nM FGF2, 97.2 nM FGFR1, and 152.8 nM FGF2−FGFR1; (G) 147.7 nM FGF2, 147.7 nM FGFR1, and 352.3 nM FGF2−FGFR1.

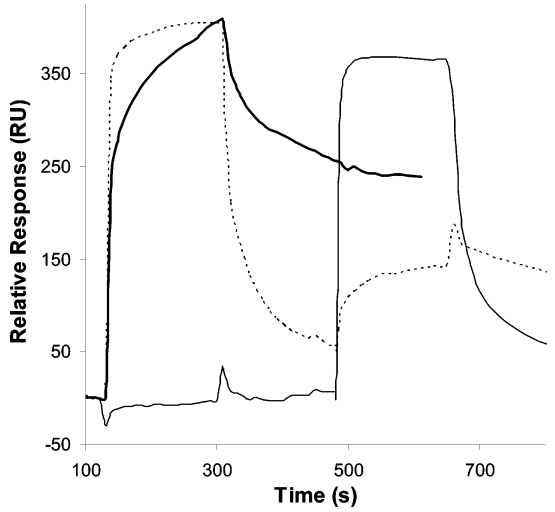

FIGURE 4: Sequential injections of FGF2 and FGFR1 as compared to an equimolar FGF2−FGFR1 injection. For the sequential injections, (---) represents 500 nM FGF2 (at 120 s) followed by 500 nM FGFR1 (at 480 s), and (—) represents 500 nM FGFR1 (at 120 s) followed by 500 nM FGF2 (at 480 s). The equimolar FGF2−FGFR1 injection (—) at 120 s consists of 147.7 nM FGF2, 147.7 nM FGFR1, and 352.3 nM FGF2−FGFR1.

s^{-1}) binding heparin (Figure 1, pathways d−e). This accounts for the formation of a stable ternary complex (Table 1). The binding affinity of FGFR1 to FGF2−heparin is nearly 22-fold greater than the binding affinity of the FGFR1/FGF2 interaction (2.7 nM as compared to 62 nM) and is consistent with the role of heparin in augmenting FGF−FGFR binding. Model 1 also accounts for the poor binding affinity of the binary FGFR1−heparin complex, despite the nine hydrogen bonds that occur between FGFR1 and heparin within one ternary complex (*9*). The crystal structure shows that all of the interactions FGFR1 makes with heparin occur with a disaccharide unit at the reducing end, which is likely to be very flexible in the absence of FGF2. Binding of FGF2 to heparin involves the segment immediately preceding the terminal disaccharide unit and will likely orient heparin to a conformation optimal for FGFR1 binding.

To test model 1, we monitored the assembly of ternary FGF2−FGFR1−heparin complex through sequential injections of FGF2 and FGFR1 and an equimolar FGF2−FGFR1 injection (Figure 4). The enhanced binding, indicated by the large (0−370) RU increase, of FGFR1 to the heparin neoproteoglycan chip following FGF2 injection (Figure 4, dashed line) contrasted to poor FGFR1 binding, associated with a nearly flat (negligible) RU response, to the neoproteoglycan prior to FGF2 injection (Figure 4, thin black line) further underscores the stepwise binding order proposed in model 1. Additionally, the similarity of the dissociation curve in the sensogram following the sequential injection of FGF2, FGFR1 (Figure 4, dashed line from 680 to 800 s) to the dissociation curve obtained from the equimolar FGF2−FGFR1 injection (Figure 4, thick black line from 320 to 600 s), as compared to the qualitatively faster dissociation curve obtained in the case of the sequential injection of FGFR1, FGF2 across the neoproteoglycan chip (Figure 4, thin black line from 680 to 800 s) suggests that stable ternary complex formation proceeds according to model 1.

Differences in the relative surface concentrations of the three different complexes formed at the sensor surface lend further credibility to model 1. The apparent values for k_a, k_d, and K_D calculated from the equimolar FGF2−FGFR1 injections onto the neoproteoglycan chip were inserted back into the ordinary differential equations to determine each interaction's contribution to the total measured response. Figure 5 reveals the amount of FGF2 bound to heparin, the amount of FGF2−FGFR1 bound to heparin, and the amount of FGFR1 bound to an FGF2−heparin complex during the first 40 s of the association phase. Most notably, the response generated at the sensor surface is primarily from stepwise formation of the ternary FGF2−FGFR1−heparin complex, whereas the response from the direct binding of the binary FGF2−FGFR1 complex to heparin accounts for only a small fraction of the total response. Close examination of the initial binding events reveals that FGF2 rapidly associates with heparin, and immediately thereafter FGFR1 binds to the preformed FGF2−heparin complex (Figure 5B). The quick binding of FGFR1 causes the surface concentration of FGF2−heparin to reach its peak in the first second and keeps FGF2−heparin from rising above 2 RU during the association phase. After 40 s, by which time the measured total response starts to approach steady-state binding levels, the contribution to the observed RU from the FGF2−FGFR1 interaction with heparin becomes negligible. Since the apparent affinity of this interaction is fairly weak, the FGF2−FGFR1 dissociates from heparin relatively easily if it is not correctly bound to form a stable ternary complex. The constant influx of fresh FGF2, FGFR1, and FGF2−FGFR1 permits FGF2 to quickly fill the site where weakly associated FGF2−FGFR1 was previously bound. Once the binary FGF2−heparin complex is formed, FGFR1 binds to form the stable FGF2−FGFR1−heparin ternary complex. This mechanism of the stepwise assembly of the ternary complex results in both a kinetic and a thermodynamic product.

In contrast, models 2 and 3 show several discrepancies with the experimental data. In model 2, an initial binary

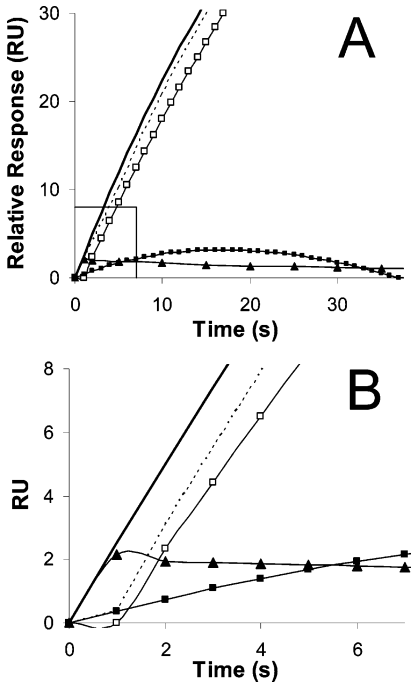

FIGURE 5: Relative surface concentrations of the complexes formed from each biomolecular interaction. Panel A examines change in RU over 35 s, and panel B is an expansion examining the initial binding events corresponding to the change in RU over the first 7 s. Response generated by each distinct complex for curve A in Figure 3 was determined using the parameters obtained from modeling the equimolar FGF2−FGFR1 injections. The amount of FGF2 bound to heparin is represented by (—▲—). The dotted line (---) shows the total amount of FGF2, FGFR1, and heparin bound together in a complex (i.e., the summation of eqs 5 and 6). The contribution from the interaction of FGF2−FGFR1 with heparin to this total surface concentration of FGF2−FGFR1−H (i.e., eq 5) is represented by (—■—). The contribution from FGFR binding to FGF2−H (eq 6) is represented by (—□—). The total response generated from the formation of all species at the sensor surface is represented by the thick black line (—).

FGF−FGFR complex precedes the formation of the ternary complex. Figure 3 shows the equimolar injection of binary FGF2−FGFR1 complex at several concentrations onto the heparin neoproteoglycan chip. At concentrations in which analyte binding to heparin is limited to FGF2, FGFR1, or FGF2−FGFR1 species, we observe binding of binary FGF2−FGFR1 to heparin occurring at a slower rate than the sequential binding of heparin to FGF2 followed by FGF2−heparin binding to FGFR1 (Table 1 and Figure 5), suggesting that ternary complex formation via model 2 is less kinetically favored than in model 1. Finally, in model 3, the binary FGFR1−HSPG complex precedes the formation of the ternary complex. This model is not supported by our data based on the poor binding affinity of the FGFR1/heparin binary interaction (K_D ~3.2 μM) (Table 1). Additionally, the data shown in Figure 4 (thin black line) also demonstrates that the prior injection of FGFR1 onto the heparin neoproteoglycan chip does not enhance the association of FGF2. Thus, model 3 is in conflict with all the experimentally observed data.

Furthermore, domain 1 of FGFR, not included in the FGFR1 employed in this study, has been shown to have autoinhibitory function that reduces the binding affinity of FGFR1 for both FGF2 and heparin (*26*, *27*). This autoinhibitory effect would have a more drastic consequence on models 2 and 3 than model 1 since FGFR binding is the initial rate-limiting step in those models. Nevertheless, we cannot exclude the possibility that on the cell surface, the kinetic and thermodynamic properties of these three pathways are different or are modulated by other regulatory factors. Hence, ternary complex formation may also occur through pathways distinct from model 1.

CONCLUSION

In summary, these data offer the first direct evidence for the stepwise order of FGF−FGFR−HSPG assembly on the cell surface. Although each of the 18 FGFs (not including FHFs) and seven FGFRs interact with varying affinity and specificity, the FGF2 and FGFR1 proteins used in this study may serve as a generalized model for the order of complex assembly. In addition to the dual role of heparin/HSPGs in augmenting FGF−FGFR binding and promoting FGFR dimerization, the proposed model for FGF−FGFR−proteoglycan assembly also supports the notion of glycosylaminoglycans (GAGs) as facilitators of intermolecular encounters between proteins (*25*). In this role, the HS-GAG chain in the cell surface HSPG would electrostatically attract FGF to the cell surface where it would concentrate. By limiting the space available to FGF2 from the three-dimensional domain of the extracellular milieu to the one-dimensional domain of the HS chain, encounters between FGF−HSPG complex and membrane bound FGFR1 are facilitated. Thus, HSPGs not only influence the thermodynamics of FGF−FGFR interactions by affording an extremely stable ternary complex but also play an active role in FGFR signaling by accelerating the kinetics of protein−protein interactions.

REFERENCES

1. Ornitz, D. M., and Itoh, N. (2001) Fibroblast growth factors, *Genome Biol. 2*, REVIEWS3005.
2. Jaye, M., Schlessinger, J., and Dionne, C. A. (1992) Fibroblast growth factor receptor tyrosine kinases: molecular analysis and signal transduction, *Biochim. Biophys. Acta 1135*, 185−99.
3. Johnson, D. E., and Williams, L. T. (1993) Structural and functional diversity in the FGF receptor multigene family, *Adv. Cancer Res. 60*, 1−41.
4. Ornitz, D. M., Xu, J., Colvin, J. S., McEwen, D. G., MacArthur, C. A., Coulier, F., Gao, G., and Goldfarb, M. (1996) Receptor specificity of the fibroblast growth factor family, *J. Biol. Chem. 271*, 15292−7.
5. Yeh, B. K., Igarashi, M., Eliseenkova, A. V., Plotnikov, A. N., Sher, I., Ron, D., Aaronson, S. A., and Mohammadi, M. (2003) Structural basis by which alternative splicing confers specificity in fibroblast growth factor receptors, *Proc. Natl. Acad. Sci. U. S. A. 100*, 2266−71.
6. Rapraeger, A. C., Krufka, A., and Olwin, B. B. (1991) Requirement of heparan sulfate for bFGF-mediated fibroblast growth and myoblast differentiation, *Science 252*, 1705−8.
7. Yayon, A., Klagsbrun, M., Esko, J. D., Leder, P., and Ornitz, D. M. (1991) Cell surface, heparin-like molecules are required for binding of basic fibroblast growth factor to its high affinity receptor, *Cell 64*, 841−8.
8. Spivak-Kroizman, T., Lemmon, M. A., Dikic, I., Ladbury, J. E., Pinchasi, D., Huang, J., Jaye, M., Crumley, G., Schlessinger, J., and Lax, I. (1994) Heparin-induced oligomerization of FGF molecules is responsible for FGF receptor dimerization, activation, and cell proliferation, *Cell 79*, 1015−24.
9. Schlessinger, J., Plotnikov, A. N., Ibrahimi, O. A., Eliseenkova, A. V., Yeh, B. K., Yayon, A., Linhardt, R. J., and Mohammadi, M. (2000) Crystal structure of a ternary FGF−FGFR−heparin complex reveals a dual role for heparin in FGFR binding and dimerization, *Mol. Cell 6*, 743−50.
10. Wu, Z. L., Zhang, L., Yabe, T., Kuberan, B., Beeler, D. L., Love, A., and Rosenberg, R. D. (2003) The Involvement of Heparan

Sulfate (HS) in FGF1/HS/FGFR1 Signaling Complex, *J. Biol. Chem. 278*, 17121−9.
11. Pellegrini, L., Burke, D. F., von Delft, F., Mulloy, B., and Blundell, T. L. (2000) Crystal structure of fibroblast growth factor receptor ectodomain bound to ligand and heparin, *Nature 407*, 1029−34.
12. Plotnikov, A. N., Schlessinger, J., Hubbard, S. R., and Mohammadi, M. (1999) Structural basis for FGF receptor dimerization and activation, *Cell 98*, 641−50.
13. Ibrahimi, O. A., Eliseenkova, A. V., Plotnikov, A. N., Yu, K., Ornitz, D. M., and Mohammadi, M. (2001) Structural basis for fibroblast growth factor receptor 2 activation in Apert syndrome, *Proc. Natl. Acad. Sci. U.S.A. 98*, 7182−7.
14. Olsen, S. K., Garbi, M., Zampieri, N., Eliseenkova, A. V., Ornitz, D. M., Goldfarb, M., and Mohammadi, M. (2003) Fibroblast growth factor (FGF) homologous factors share structural but not functional homology with FGFs, *J. Biol. Chem. 278*, 34226−36.
15. Zhang, F., Fath, M., Marks, R., and Linhardt, R. J. (2002) A highly stable covalent conjugated heparin biochip for heparin−protein interactions studies, *Anal. Biochem. 304*, 271−3.
16. Ibrahimi, O. A., Zhang, F., Eliseenkova, A. V., Linhardt, R. J., and Mohammadi, M. (2004) Proline to arginine mutations in FGF receptors 1 and 3 result in Pfeiffer and Muenke craniosynostosis syndromes through enhancement of FGF binding affinity, *Hum. Mol. Genet. 13*, 69−78.
17. Goldstein, B., Coombs, D., He, X. Y., Pineda, A. R., and Wofsy, C. (1999) The influence of transport on the kinetics of binding to surface receptors: application to cells and BIAcore, *J. Mol. Recognit. 12*, 293−9.
18. Kinsella, L., Chen, H. L., Smith, J. A., Rudland, P. S., and Fernig, D. G. (1998) Interactions of putative heparin-binding domains of basic fibroblast growth factor and its receptor, FGFR-1, with heparin using synthetic peptides, *Glycoconj. J. 15*, 419−22.
19. Delehedde, M., Lyon, M., Gallagher, J. T., Rudland, P. S., and Fernig, D. G. (2002) Fibroblast growth factor-2 binds to small heparin-derived oligosaccharides and stimulates a sustained phosphorylation of p42/44 mitogen-activated protein kinase and proliferation of rat mammary fibroblasts, *Biochem. J. 366*, 235−44.
20. Powell, A. K., Fernig, D. G., and Turnbull, J. E. (2002) Fibroblast growth factor receptors 1 and 2 interact differently with heparin/heparan sulfate. Implications for dynamic assembly of a ternary signaling complex, *J. Biol. Chem. 277*, 28554−63.
21. Pantoliano, M. W., Horlick, R. A., Springer, B. A., Van Dyk, D. E., Tobery, T., Wetmore, D. R., Lear, J. D., Nahapetian, A. T., Bradley, J. D., and Sisk, W. P. (1994) *Biochemistry 33*, 10229−48.
22. Neufeld, G., and Gospodarowicz, D. (1985) The identification and partial characterization of the fibroblast growth factor receptor of baby hamster kidney cells, *J. Biol. Chem. 260*, 13860−8.
23. Moscatelli, D. (1987) High and low affinity binding sites for basic fibroblast growth factor on cultured cells: absence of a role for low affinity binding in the stimulation of plasminogen activator production by bovine capillary endothelial cells, *J. Cell Physiol. 131*, 123−30.
24. Nugent, M. A., and Edelman, E. R. (1992) Kinetics of basic fibroblast growth factor binding to its receptor and heparan sulfate proteoglycan: a mechanism for cooperactivity, *Biochemistry 31*, 8876−83.
25. Lander, A. D. (1998) Proteoglycans: master regulators of molecular encounter? *Matrix Biol. 17*, 465−72.
26. Wang, F., Kan, M., Yan, G., Xu, J., and McKeehan, W. L. (1995) Alternately spliced NH2-terminal immunoglobulin-like Loop I in the ectodomain of the fibroblast growth factor (FGF) receptor 1 lowers affinity for both heparin and FGF-1, *J. Biol. Chem. 270*, 10231−5.
27. Olsen, S. K., Ibrahimi, O. A., Raucci, A., Zhang, F., Eliseenkova, A. V., Yayon, A., Basilico, C., Linhardt, R. J., Schlessinger, J., and Mohammadi, M. (2004) Insights into the molecular basis for FGF receptor autoinhibition and ligand binding promiscuity, *Proc. Natl. Acad. Sci. U.S.A.*, *101*, 935−940.

BI0352320